JOURNAL OF MATERIALS SCIENCE **38** (2003) 941 – 952

Microstructure-property studies in friction-stir welded, Thixomolded magnesium alloy AM60

J. A. ESPARZA, W. C. DAVIS, L. E. MURR
Department of Metallurgical and Materials Engineering, University of Texas at El Paso, El Paso, TX 79968, USA

Thixomolded* magnesium alloy AM60 plates joined by friction-stir welding were observed to be as strong or stronger than the unwelded base material. The thixotropic microstructures of the as-molded plates consisted of either 3% or 18% primary solid fraction of α-Mg globules ($\sim$45 μm average size) in a eutectic mixture consisting of α-Mg grains ($\sim$10 μm) surrounded by $Mg_{17}Al_{12}$ intermetallic grains in the α-Mg grain boundaries (having an average size of 1–2 μm). This complex, composite microstructure became a homogeneous (Mg + 6% Al)), recrystallized, equiaxed grain (10–15 μm) microstructure in the weld zone. © *2003 Kluwer Academic Publishers*

1. Introduction

The use of magnesium alloys is growing rapidly in areas such as consumer electronics, automotive and aerospace applications, and injection-molded plastic consumer product substitutions; especially where temperature and electrical properties become important and/or limiting conditions in production or use. Magnesium alloys also possess high specific strength and stiffness, very low density (roughly 30% lighter than aluminum), good thermal conductivity, and electromagnetic interference shielding capabilities. The development of new processes, such a thixomolding, allow for low-cost, environmentally attractive production of complex, net-shape, and thin-walled parts. The thixomolding process combines aspects of plastic injection molding with those of die casting [1]. Room temperature magnesium alloy pellets or fragments are fed into a heated barrel containing an argon atmosphere to prevent oxidation. A screw rotation system moves the magnesium alloy fragments or chips forward through the barrel, which is heated in roughly 10 temperature zones to bring the temperature to the semi-solid or thixotropic regime; roughly 100°C below the actual melting temperature. The screw action noted shears and rounds the growing dendrites to create a thixotropic slurry consisting of essentially spheroidal, globular solid particles in a continuous liquid matrix which is injected into a preheated metal mold to produce a net shape part. No external foundry or molten metal handling is necessary, eliminating the use of SF_6 as a common cover gas. There is no flux, and any scrap is easily recycled. The prospects for explosion are eliminated. Magnesium alloys are also easily oxidized in conventional casting and fusion welding applications. Consequently, the application of friction-stir welding to joining magnesium or magnesium alloy parts can eliminate this prospect and provide an efficient joining process.

Friction-stir welding (FSW) has been demonstrated to be a very effective and environmentally attractive method for joining a wide range of metals and alloys [2–4]. The process involves severe plastic deformation in the solid state; there is no melting and metal flow occurs by dynamic recrystallization. Magnesium alloys such as AZ31B have been demonstrated to be successfully joined by FSW [5, 6] and Nakata *et al.* [7] have recently reported on the FSW of thixomolded sheet of magnesium alloy AZ91D (Mg 9% Al, 1% Zn). Dynamic recrystallization provides the mechanism for solid-state flow in the FSW process and the weld zone is always characterized by a recrystallized, usually equiaxed, small grain structure. In some cases this recrystallized regime exhibits superplastic behavior [8, 9]. When consistently and contiguously exposed to FSW, a volume of material can in effect be reprocessed to exhibit a residual, homogeneous, recrystallized, fine-grain structure [4, 9, 10]; often referred to as friction-stir processing (FSP).

In this study we explored the joining of various thixomolded AM-60 magnesium alloys by FSW as a continuous, environmentally sound production and assembly process. This study especially characterized and compared the microstructures of the thixomolded base metals with those of the residual FSW zones utilizing optical metallography and transmission electron microscopy (TEM). Microhardness profiles through the joined sections and corresponding tensile test data were also correlated with these microstructures.

2. Experimental

Thixomolded, flat panels or plates nominally 0.2 cm thick of magnesium alloy AM60B (6% Al, 0.3% Mn, balance Mg in weight percent) were prepared with low and high solid fractions of primary phase (α-Mg) to

*Thixomolding and Thixomolded are registered trademarks of Thixomat Inc., Ann Arbor, MI, USA.

evaluate the role of the solid fraction on FSW efficiency. The experimental solid fractions were nominally 3% and 18% and exhibited average porosities of 1.5%. However the actual solid fractions in samples examined ranged from 2 to 5% for the low fraction to 15 to 20% high fraction. These experimental panels were provided by Thixomat, Inc., Ann Arbor, MI (USA).

The tool assembly for FSW consisted of a 0.19 cm long, standard 1/4-20 01 tool-steel screw nib heat treated to a Rockwell C hardness of 62; with essentially only one right-handed thread; nominally 0.63 cm in diameter. The nib or head-pin (HP) tool was mounted in a 1.9 cm diameter milling chuck in a modified Gordon-Mastermill milling machine. The head-pin (tool) rotation direction was counter-clockwise and an optimized rotation speed (R) was found to be 2000 rpm; at a weld or traverse (T) speed of 2 mm/s (Fig. 1). This rotation speed was higher than normal welding tool rotation speeds for thicker work pieces ($\geq$0.64 cm) which are usually around 500 to 1000 rpm. Generally, tool rotation speeds increase for decreasing work piece thicknesses.

Following friction-stir welding (FSW), sections were cut from the weld face (Fig. 1) and polished and etched. The Mg alloy samples were polished with a solution of 10 mL nitric acid and 90 mL methanol. The polished surfaces were etched with a solution of 70 mL picral (10 g picric acid in 100 mL ethanol), 10 mL acetic acid, and 10 mL water; with fresh picral blotted repeatedly onto the surface to prevent residue buildup. Following examination of polished and etched surfaces by optical metallography, surface areas were also observed

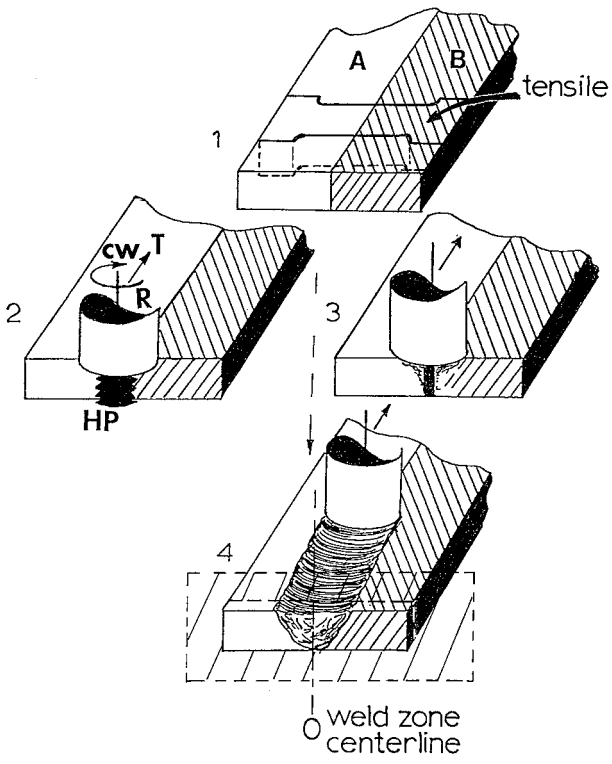

Figure 1 Friction-stir weld schematic showing welding parameters. With a counter-clockwise rotation, the shaded side advances into the unshaded side. The right side of the weld (4) is therefore the advancing side. The tool (or head-pin) is designated HP. In (1) tensile refers to the tensile specimen configuration for workpiece and FSW specimens. In (4) the dotted plane illustrates the FSW section.

in a scanning electron microscope (SEM) (operated at 20 kV) fitted with an EDAX energy-dispersive X-ray (EDX) spectrometer system. This allowed for microchemical characterization of the various phase regimes and to examine the compositions averaged over specific areas of the weld region or the work piece regime.

Thin specimens for transmission electron microscopy (TEM) were sliced from the base metal (or work pieces) and the weld zones (Fig. 1) in the same manner as polished sections were prepared, and then polished to $\sim$0.2 mm sections and 3 mm disks punched from them. Final polishing of the 3 mm disks in a Tenupol dual jet electropolishing unit to produce electron transparent thin sections used a solution of nitric acid and methanol at room temperature. The solution composition was 50 mL nitric acid and 1.2 L methanol in the weld zone and 75 mL nitric acid and 1.2 L methanol in the base metal. No current (or voltage) was applied. A Hitachi H-8000 analytical TEM employing a goniometer-tilt stage and fitted with a Noran energy-dispersive X-ray spectrometer was operated at 200 kV accelerating potential in the examination of the thinned samples.

Vickers microhardness measurements were made near the mid-thickness for welded sections; extending from the as-molded base metal through the FSW zone (Fig. 1). A 50 gf ($\sim$0.5 N) load was utilized in a Shimadzu digital hardness tester. The corresponding mechanical properties (tensile properties) were measured by cutting standardized tensile specimens from the surface plane (perpendicular to the microhardness reference plane) as shown in Fig. 1(1). Tensile specimens measured 10 cm in length, 2.5 cm wide at the grips, and a reduced cross-section of 1.25 cm width in a gauge length of 5 cm; having a connecting radius of 0.3 cm. This is a modification of ASTM standard E8. The specimen thickness was milled and polished nominally to 1.5 mm. Tensile tests were performed in an Instron 1127 universal tensile machine at a cross-head speed of 0.3 mm/min.

3. Results and discussion

Fig. 2 shows typical weld cross sections for the low solid fraction (3%) (Fig. 2a) and high solid fraction (18%) (Fig. 2c) AM60 alloy. The base material or starting work pieces shown on either side of the weld exhibit typical thixotropic features. The unmelted fraction of the alloy, termed a primary solid fraction, is surrounded by the alloy transformation product in a liquid state at the processing temperature. In addition to the large primary solid fraction or α-Mg solid solution globules (which range in size from 10 to 200 μm; with an average size of $\sim$45 μm) there is a much smaller α-Mg distribution composing the surrounding eutectic matrix (imaged as white dots in Fig. 2) which is a mixture of α-Mg and an intermetallic $Mg_{17}Al_{12}$; with the α-Mg phase grains essentially surrounded by the intermetallic (in the α-Mg grain boundaries). The intermetallic is also composed of grains less than 1 μm in size. These features are illustrated with greater clarity in Figs 3 and 4. Fig. 3 shows that while the larger (primary) solid,

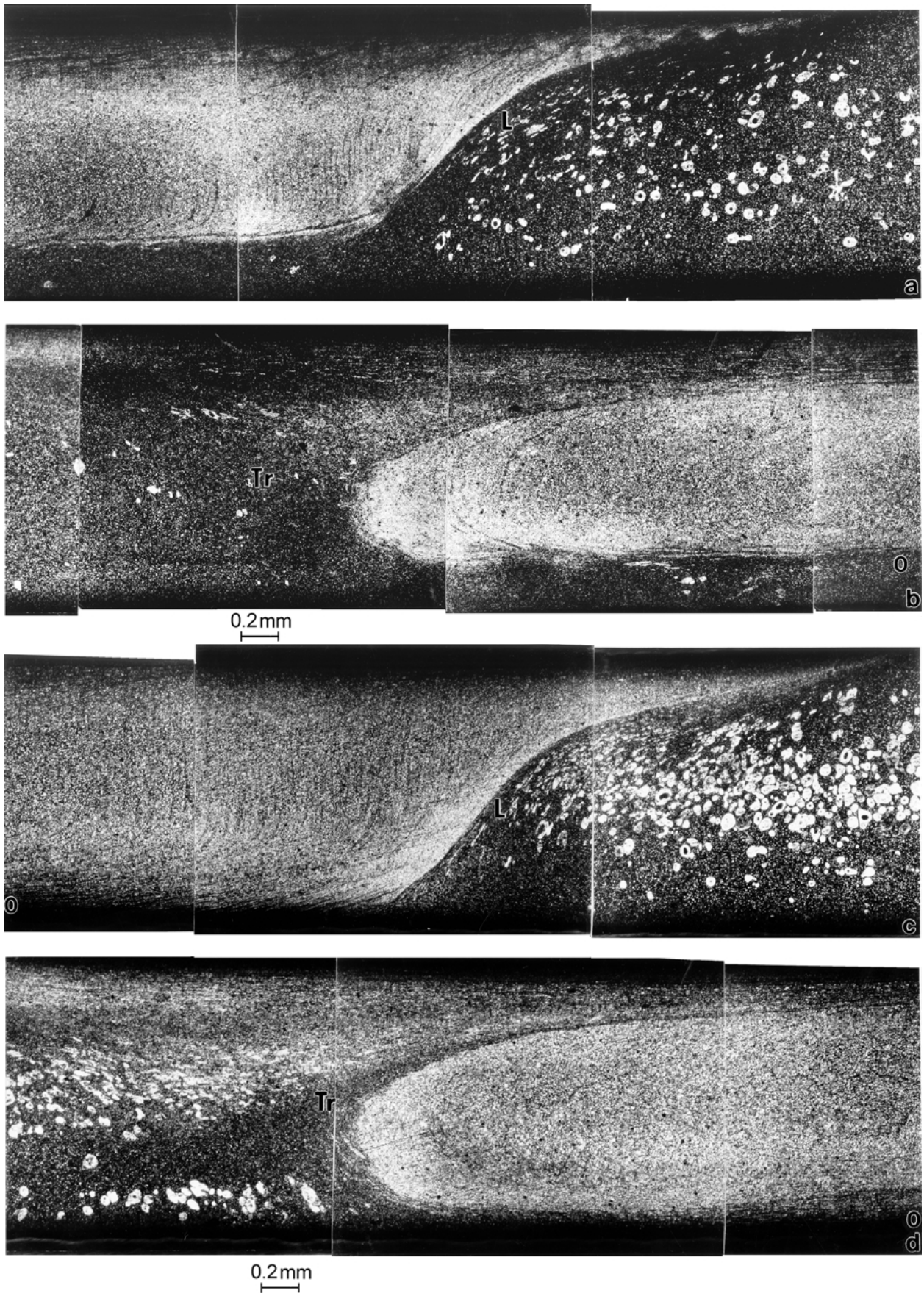

Figure 2 Weld cross-section views. (a) and (b) show advancing (leading, L) half and receding (trailing, Tr) half respectively for the 3% solid fraction, (c) and (d) show leading half and trailing half respectively for the 18% solid fraction. The advancing or leading edge of the weld is on the right side (indicated L) and characterized by a sharp transition to the weld zone. The trailing edge (Tr) is diffuse by contrast. There is a stir affected and heat affected zone outside these transitions and extending into the workpiece. The half weld sections shown are referenced to the approximate weld center line (0) shown schematically in Fig. 1(4).

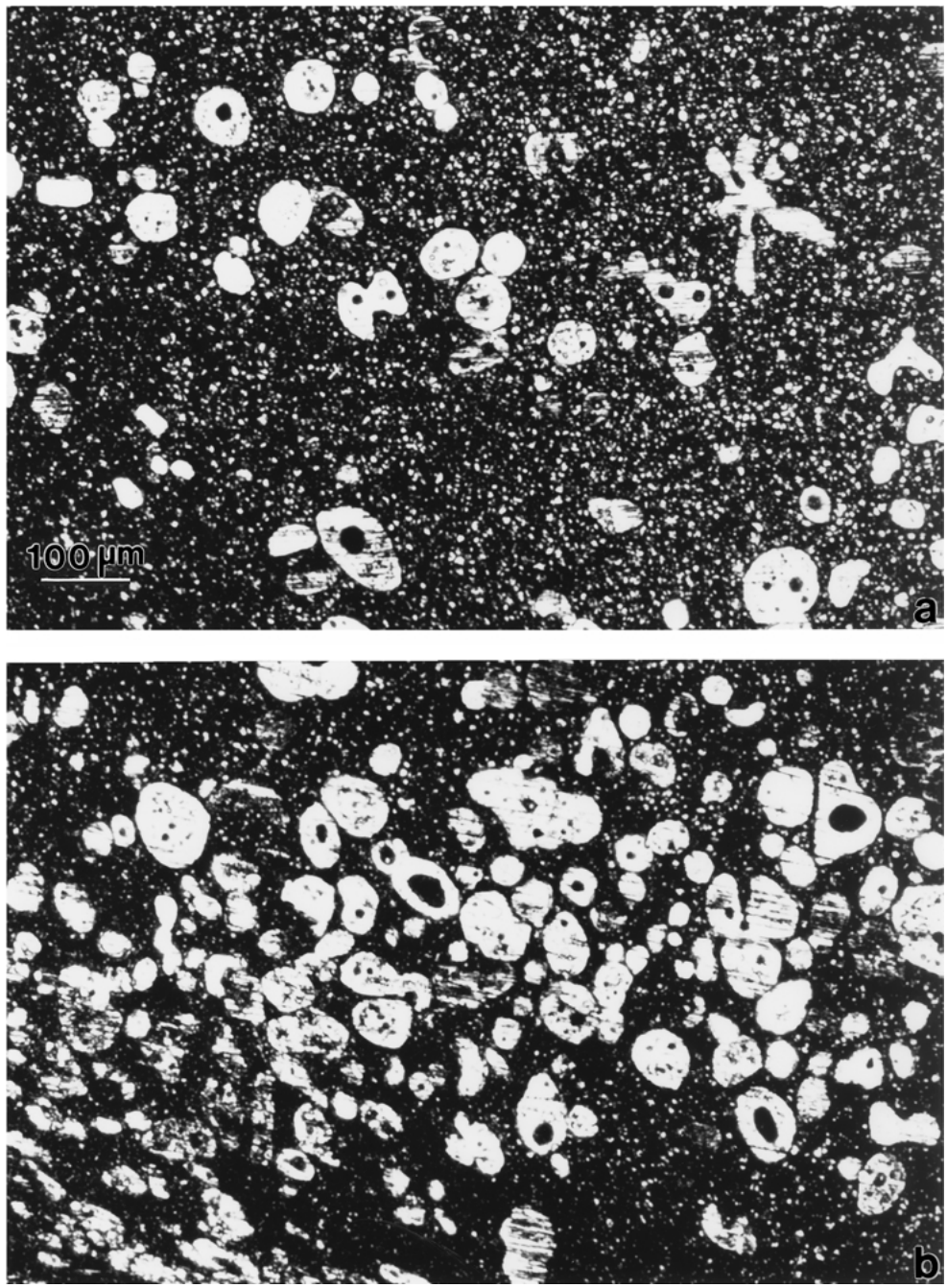

Figure 3 Optical metallography images of the thixomolded/thixotropic microstructure. (a) 3% solid fraction (primary phase). (b) 18% solid fraction (primary phase). The primary phase is white.

globular fraction is roughly 3% in Fig. 3a, the refined α-Mg phase in the matrix has a higher volume than the same phase refinement in the high solid fraction material shown in Fig. 3b. As a consequence, the eutectic mixture is somewhat different in comparing Fig. 3a and b. Fig. 4 shows these differences in more detail; especially comparing Fig. 4a and b with Fig. 4c and d respectively. Fig. 4a and c also illustrate that many of the large (primary) α-Mg particles contain deformation twins. Many of these particles also contain precipitates in their interiors with predominantly spherical shapes. These originate by spheroidization, melting, and resolidification of the low melting fraction of the alloy entrapped within the solid particles as a consequence of chemical (elemental) segregation. Fig. 5 shows magnified views of these entrapped, solidification product for both the low solid fraction (3%) (Fig. 5a) and the high solid fraction (18%) (Fig. 5b) of α-Mg. Fig. 5 also contains several EDX spectra inserts which attest to the variations in chemistry and corresponding phase microstructures for both the primary α-Mg globules and the eutectic matrix. Fig. 5a shows a portion of a primary α-Mg globule containing a solidified product region and surrounded by the eutectic matrix. The matrix morphology consists of fairly regular grains of α-Mg surrounded by the intermetallic (in the grain boundaries). As shown by the EDX spectrum (1) in Fig. 5a, the α-Mg grains, including the primary fraction, tend to contain only Mg near their centers; with the Al content increasing outward. This is a characteristic of die cast AM60 as well. When a larger area is scanned as shown in EDX spectrum (2) in Fig. 5a, the base (average) AM60 composition is observed to vary from about 5 to 7% Al. The α-Mg grains in the matrix of Fig. 4b and

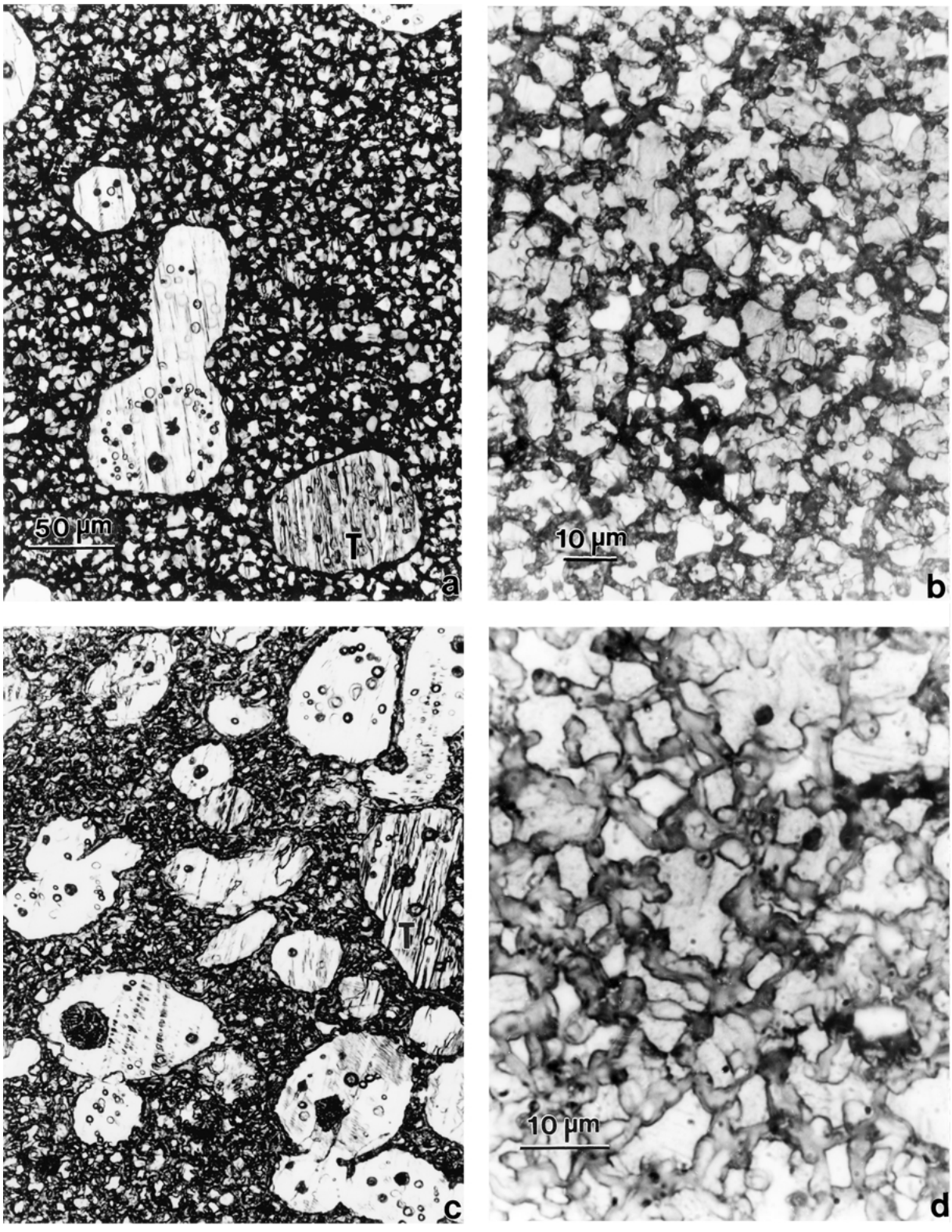

Figure 4 Enlarged views of the primary phase and eutectic matrix microstructures. (a) Primary phase and matrix for 3% solid fraction. (b) Eutectic matrix mixture for 3% solid fraction. (c) Primary phase and matrix for 18% solid fraction. (d) Eutectic matrix mixture for 18% solid fraction. Deformation twins are marked T in (a) and (c). Magnification in (c) is indicated in (a).

5a vary in size from roughly 2 μm to 15 μm; with an average size of 10 μm. The surrounding intermetallic phase regime varies from 1–2 μm thick. Fig. 5b shows a larger aluminum fraction within the solidified inclusion in EDX spectrum (3). Quantification analysis of the characteristic X-ray data (spectrum (3)) indicated roughly 82% Mg, 17% Al, and 1% Mn. It can be observed in both Fig. 5a and b that the solidified inclusion is also composed of the eutectic mixture: α-Mg + the intermetallic. It can be observed on comparing Fig. 4b and d that the morphology of the eutectic mixture or matrix structure is slightly different in the low and high primary fraction materials.

A recent, detailed analysis correlating microstructures and properties of a thixomolded AZ91D magnesium alloy (9% Al, 1% Zn, balance Mg) by Czerwinski *et al*. [11] drew conclusions very similar to those implicit in Figs 3 to 5, and the associated discussion above.

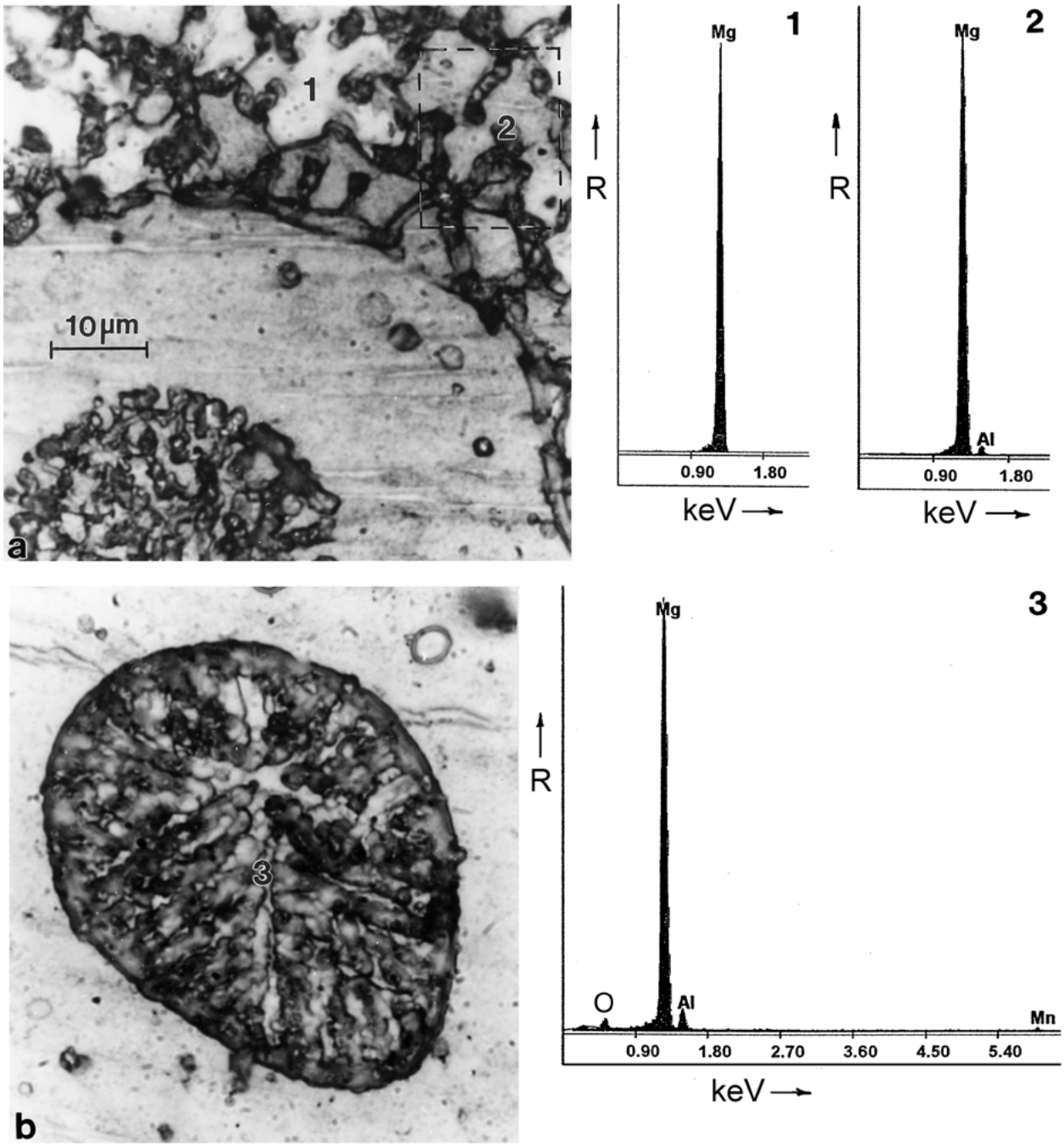

Figure 5 Entrapped solidification features and corresponding microstructures. (a) 3% solid fraction showing solidification zone in primary α-Mg globule and surrounding matrix mixture of α-Mg grains and grain boundary intermetallic $Mg_{17}Al_{12}$. (b) Occluded solidification zone in α-Mg primary phase globule in 18% solid fraction sample. EDX spectra inserts illustrate typical chemistries and chemical element variations at corresponding numbers. Note oxygen peak in (3).

Fig. 6 compares the microstructures for the weld zone centers in Fig. 2. In contrast to the base microstructures shown in Figs 3 and 4, the weld zone microstructures are observed to consist of relatively equi-sized grains with a homogeneous composition characteristic of AM60 (Mg + 6% Al). This is illustrated in the EDX spectrum insert in Fig. 6a where the quantification software indicated 93% Mg and 7% Al. The equiaxed, homogeneous, grain structure of the weld zones shown in Fig. 6 are characteristic of the weld zone microstructure recently observed for the FSW of magnesium alloy AZ31B (3% Al, 1% Zn, balance Mg) [6]. This microstructure results by dynamic recrystallization and grain growth.

It might be noted that there is a very slight but apparent difference in the weld zone grain sizes on comparing Fig. 6a and b. For the FSW of the 3% solid fraction (Fig. 6a), the weld zone grain size ranged from roughly 1 to 25 μm; the same for the 18% solid fraction (Fig. 6b). However, the average grain size for the low solid fraction was 10 μm while for the high fraction it was 15 μm. The slightly larger grain size may be due to a slightly higher weld temperature. Although weld temperatures were not measured specifically, recent measurements in aluminum alloy systems indicate maximum center-line temperatures of $0.8T_M$, where T_M is the melting temperature [12]. The solid solubility of Al at this temperature is about 10 atomic percent.

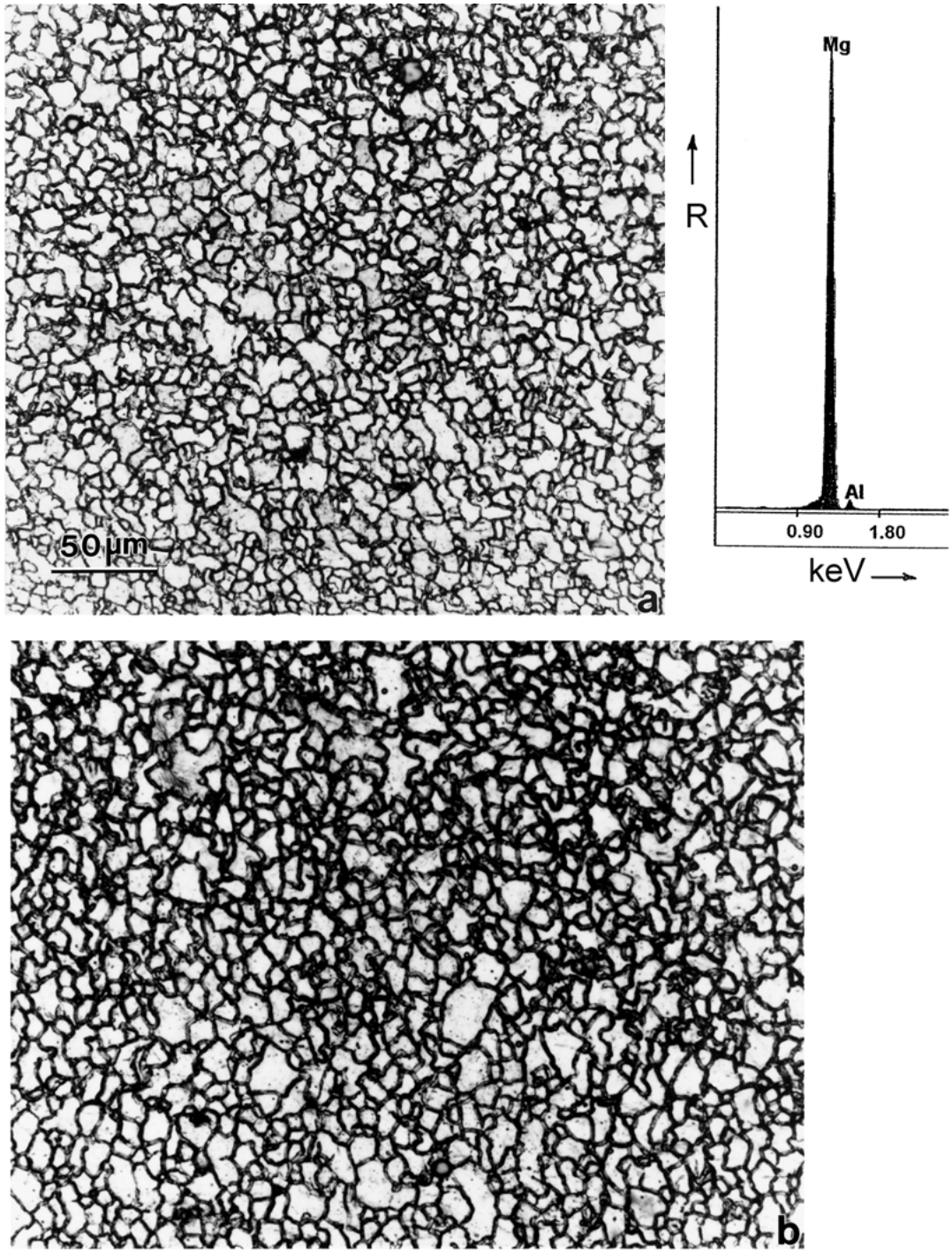

Figure 6 Examples of weld zone center microstructures. (a) 3% primary solid fraction, (b) 18% primary solid fraction. The EDX spectrum insert in (a) illustrates a typical area scan.

It is also apparent in Fig. 6 that the α-Mg solid solution (Mg + 6% Al) grains are not surrounded by a "film" of intermetallic phase and there do not appear to be any observable intermetallic precipitates of $Mg_{17}Al_{12}$. These microstructural features and a comparison of microstructural details are illustrated in the TEM images and selected-area electron diffraction (SAED) pattern inserts in Figs 7 and 8, for the low fraction solids and high fraction solids samples, respectively. Fig. 7 shows several examples of TEM bright-field images of both the base microstructure and the weld zone microstructure for the low (3%) solid fraction sample. Fig. 7a shows a large intermetallic grain separating an α-Mg grain. The SAED pattern insert in Fig. 7a illustrates α-Mg hcp solid solution Mg + 6% Al ($a \cong 3.18$ Å, $c \cong 5.14$ Å) [13] reflections with superimposed $Mg_{17}Al_{12}$ reflections (see JCPDS-ICOD #1-1128 where the patterns can be indexed with $a = 10.56$ Å). The large strongly diffracting intermetallic phase also contains a high density of defects; mostly dislocations. Fig. 7b shows a weld section with a (0001) grain component. The dislocation density seems to be considerably reduced in contrast to Fig. 7a. Fig. 7c shows another example of the FSW zone microstructure with reduced dislocation density and a relatively clean grain boundary separating the α-Mg alloy grains (arrows). The grain orientation in Fig. 7c illustrated by the SAED pattern insert is also coincident with (0001).

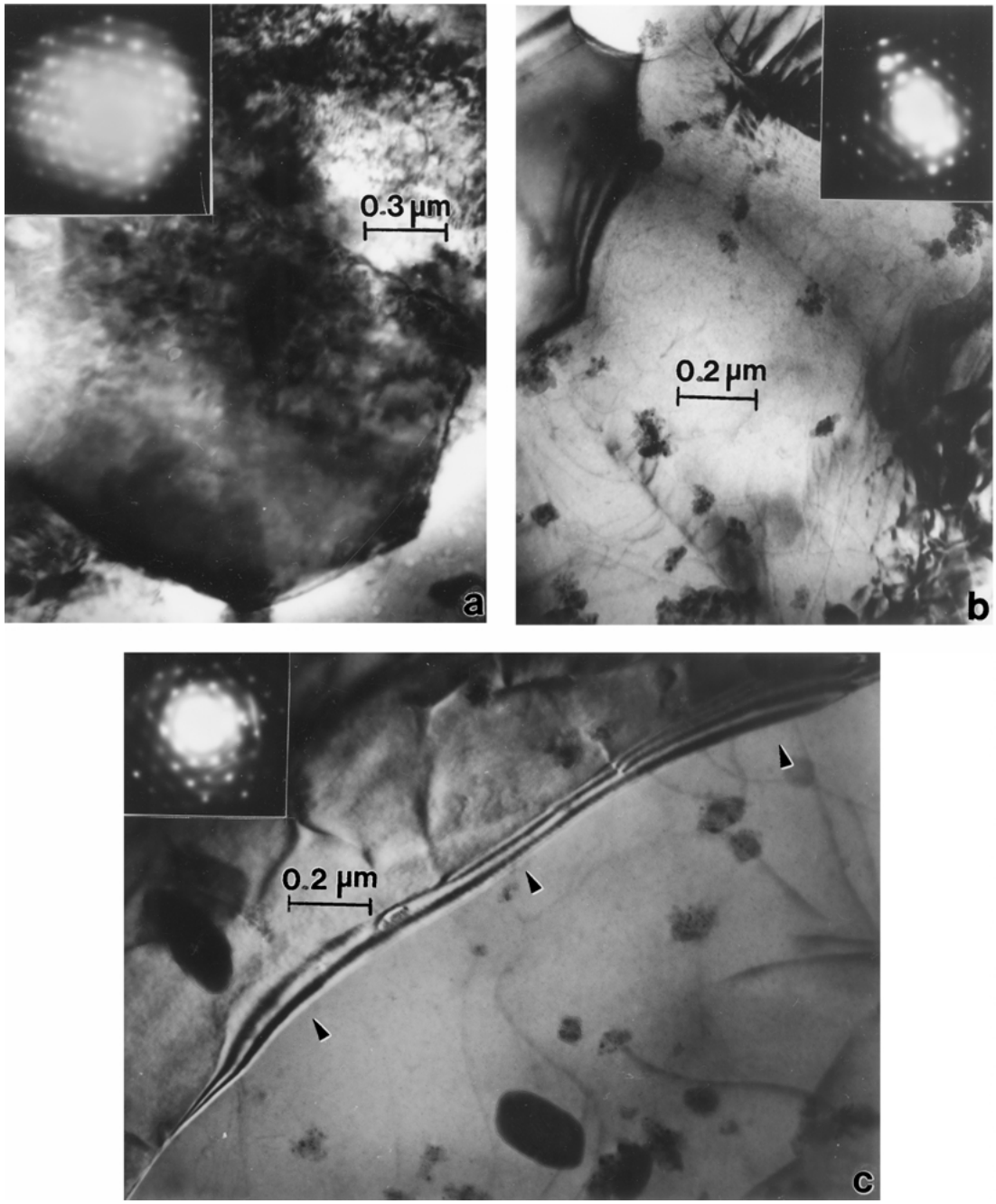

Figure 7 TEM bright-field images and representative SAED pattern inserts for samples containing 3% of the primary solid. (a) and (b) show examples of the base-workpiece region. (c) Weld zone region. Grain boundary is noted by arrows. Zone axis in (a) to (c) is [0001]. The $Mg_{17}Al_{12}$ zone axis in (a) is [112]. The operating reflection in (c) is $\mathbf{g} = [10\bar{1}2]$ and the corresponding extinction distance for grain boundary fringes is $\sim$0.13 μm.

Fig. 8 shows, for comparison with Fig. 7, some examples of TEM microstructure images for the high (18%) solid fraction sample. Fig. 8a and b show two examples of α-Mg microstructures in the base material. Fig. 8a exhibits a high density of dislocations for a (0001) grain surface orientation while Fig. 8b shows several deformation twins in a (0001) orientation. There is also a high density of dislocations even within the twins. Fig. 8c shows a (0001) grain in the FSW zone with some dislocations and Moire fringe patterns (arrow) [14]. It is also noted in Fig. 8c that, similar to Fig. 7c, the grain boundaries do not contain any significant evidence for intermetallic precipitation; confirming the conclusion that the FSW process produces equi-sized, homogeneous grains by dynamic recrystallization.

Previous FSW studies in many aluminum alloys [15–19] and other materials, including dissimilar materials [19–21] and aluminum metal-matrix composites (MMC's) [21, 22] have illustrated the weld zone microstructures to be characterized by dynamic recrystallization and grain growth. Adiabatic temperatures have been measured in the FSW of 6061 aluminum to be as high as 0.8 T_M (where T_M is the melting temperature) [12]. Consequently, for corresponding temperature effects (or temperatures above about 370°C) in the FSW of the thixomolded AM60 samples, the intermetallic phase would be expected to dissolve and result in a homogeneous, AM60 composition as indicated in the EDX spectrum insert in Fig. 6a.

It can be observed in retrospect by re-examining Figs 2 to 6 that the most apparent microstructural

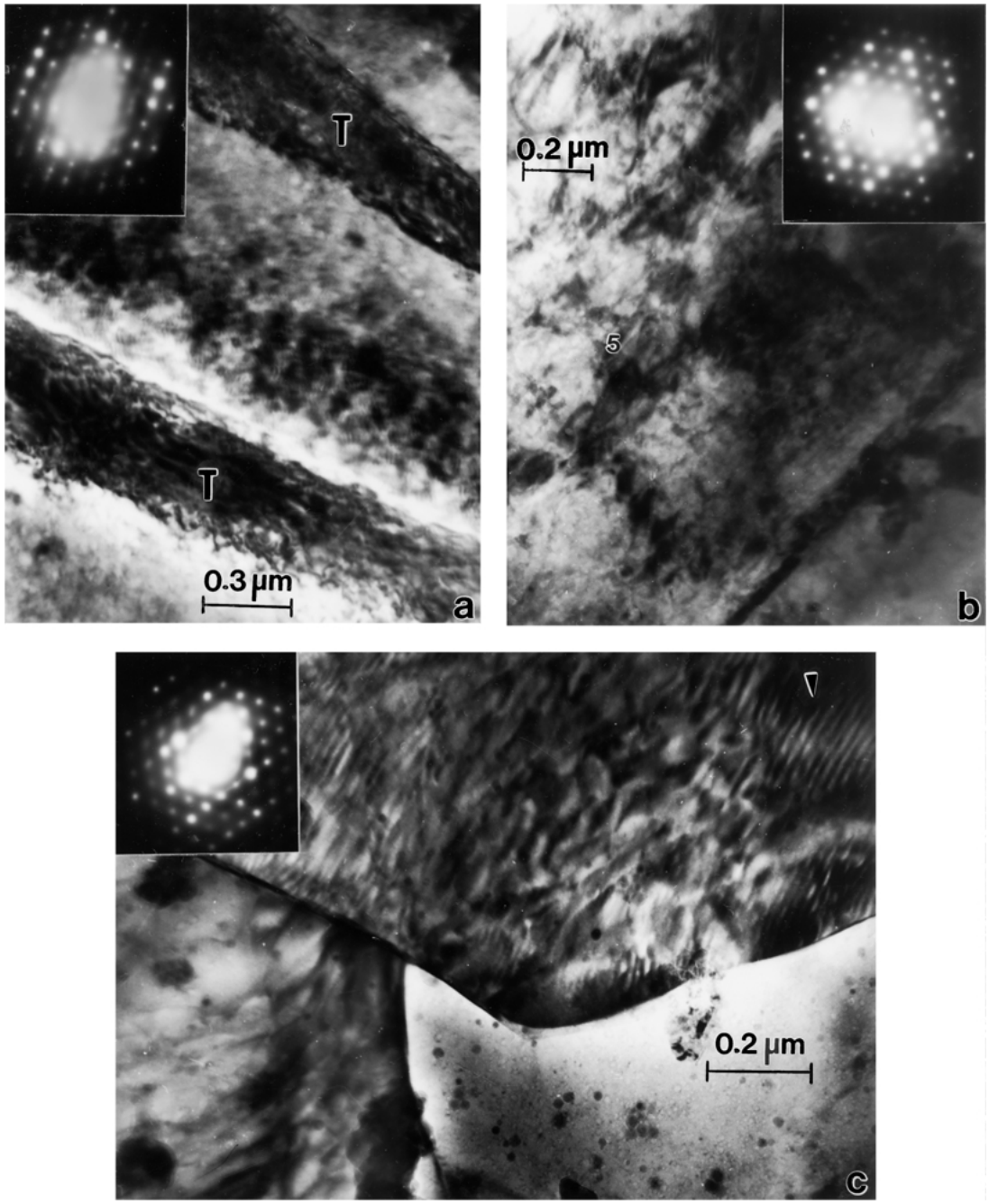

Figure 8 TEM bright-field images and representative SAED pattern inserts for samples containing 18% of the primary solid. (a) and (b) show examples of the base-workpiece region. (c) Weld zone region. Deformation twins are marked T in (b). Arrow in (c) shows Moire fringes. The zone axis in all cases indicated by SAED pattern inserts is [0001]. The operating reflections in (b) and (c) are $\mathbf{g} = [0\bar{2}20]$ and $\mathbf{g} = [\bar{2}200]$ respectively.

distinction between the two different work piece plates is the primary (solid) fraction of α-Mg globules although some difference exists for the eutectic matrix as well. There is little difference between the residual weld zone microstructures but of course there is a considerable difference between the eutectic matrix and the weld zone, although the range of α-Mg grain sizes and average grain sizes for the work piece plates and the weld zones does not vary significantly. Figs 7 and 8 show a corresponding reduction in the weld zone dislocation density.

Fig. 9 shows typical microhardness profiles through the two different weld zones to be very similar. The average base hardness for the 3% solid fraction sample was HV62 in contrast to HV55 for the 18% solid fraction sample; a reduction of roughly 10%. The average weld zone hardness was slightly elevated relative to the base hardness for both materials although the high (18%) solid fraction sample exhibited a slightly reduced hardness on the right or leading edge of the weld; corresponding to a heat affected regime lowering the solid fraction as illustrated in Fig. 2b. This is essentially the same observation as that reported by Nakata *et al*. [7] for FSW of thixomolded AZ91D. The base hardness range is also similar to that observed for thixomolded AZ91D plates by Czerwinski *et al*. [11] where they noted that in this alloy (AZ91D) the magnesium matrix was more susceptible to deformation than the intermetallic phase, which was nearly 3 times harder. However, there was not any significant hardness scatter as evident from the hardness profile data reproduced in Fig. 9, and the intermetallic seemed

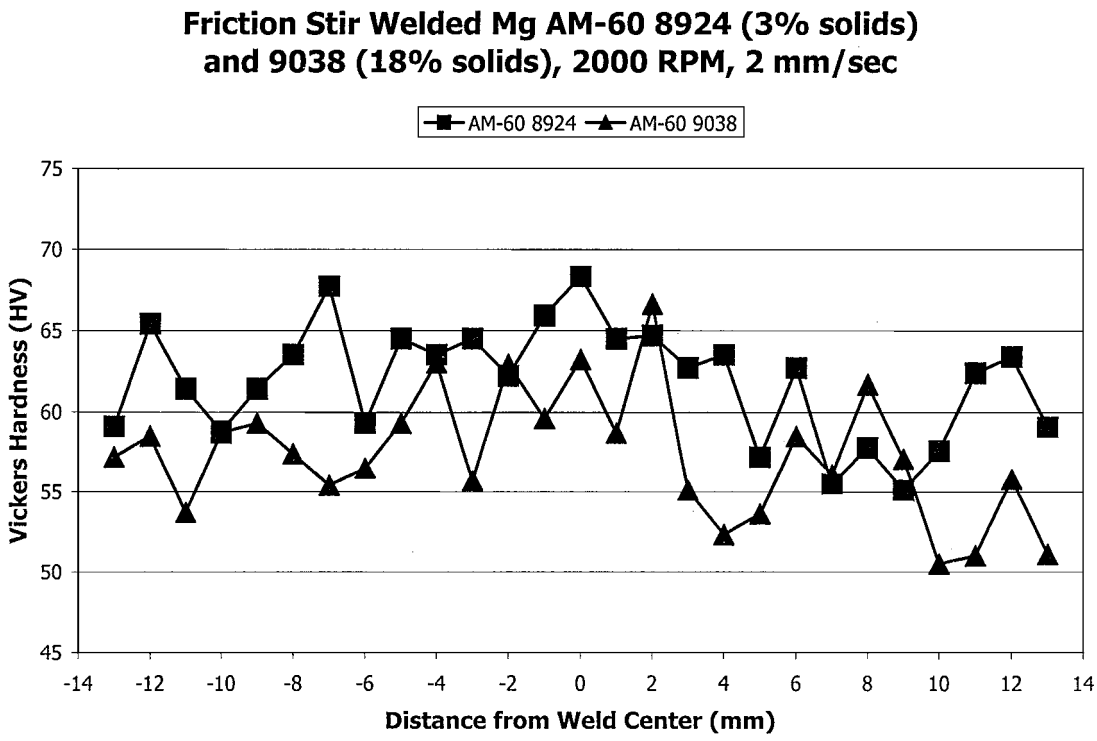

Figure 9 Residual Vickers microhardness profiles across the weld face (Figs 1a and 2). 8924 and 9038 indicate corresponding production codes for the 3% (squares) and 18% (triangles) solid fraction of primary phase respectively.

to contain a high dislocation density as illustrated in Fig. 7a.

Table I compares the corresponding tensile data for the two different solid fraction base plates and welded plates. Overall, the weld zones (or the FSW samples) respond very similar to the base material and in the case of the high fraction solids sample (18% solid fraction) the FSW sample has a recognizably higher yield stress and hardness, although it is consistent for both the base and FSW samples for the low solid fraction (3%); and the yield stress/hardness ratio for all samples varies only between 0.19 and 0.22. The ultimate tensile strength for both FSW samples is less than 10% below the base material samples and probably results because of variations in the microstructure between the weld zone and the base material in the stir-affected and heat-affected zone (sometimes referred to as a thermo-mechanically affected zone) since this is where the fracture occurs in the FSW samples. Base metal fracture also occurred for FSW of thixomolded AZ91D sheet [7]. Fig. 10 illustrates a typical SEM fractograph for a high fraction (18%) sample which fractured just outside the weld zone. There is a relatively high fraction of ductile-dimple structure within the eutectic matrix and decohesion between the primary (α-Mg) globules and the matrix (arrow in Fig. 10). There appears to be some flat areas corresponding to decohesion at the intermetallic, but these phases are on the same size range as the ductile dimple structure.

The elongation for the low (3%) solid fraction samples (both base and FSW) was 5% while 4% for the high (18%) fraction FSW sample and 8% for the base material. In recent work on thixomolded AZ91D by Czerwinski *et al.* [11] they observed an elongation of roughly 4.5% between 2 and 20% solid fraction while Ghosh *et al.* [23] observed elongations of 7.5% at 2% solid fraction and 4.5% elongation at 20% solid fraction. However, the thixomolded AZ91D had ultimate tensile strengths which varied between about 275 MPa and 240 MPa from 2% to 20% solid fraction of the primary (α-Mg) phase [11, 23]. Nakata *et al.* [7] noted that the tensile strength of the FSW zone in thixomolded AZ91D sheet was roughly 40% higher than the base material. In spite of the variability of the thixomolded

TABLE I Thixomolded AM60 tensile data[a]

Solid fraction (α-Mg) sample	Yield stress σ_y (MPa) (0.2% offset)	Hardness (HV, MPa)[b]	σ_y (HV)	Ultimate tensile strength UTS (MPa)	Elongation (%)[c]
3%-Base	135	620	0.22	210	5
3%-FSW	135	640	0.21	195	5
18%-Base	105	550	0.19	210	8
18%-FSW	135	620	0.22	192	4

[a]Strain rate of 2×10^{-3} s^{-1} @ 22°C. Best or averaged test data is shown for the base or unwelded workpieces, and specimens cut from the FSW samples as illustrated in Fig. 1.
[b]Vickers hardness (HV) (average) from Fig. 9. Vickers hardness number $\times$ 10 is equivalent to units in MPa.
[c]Elongation is percent strain to fracture. Fracture always occurred out of the weld zone for the FSW samples.

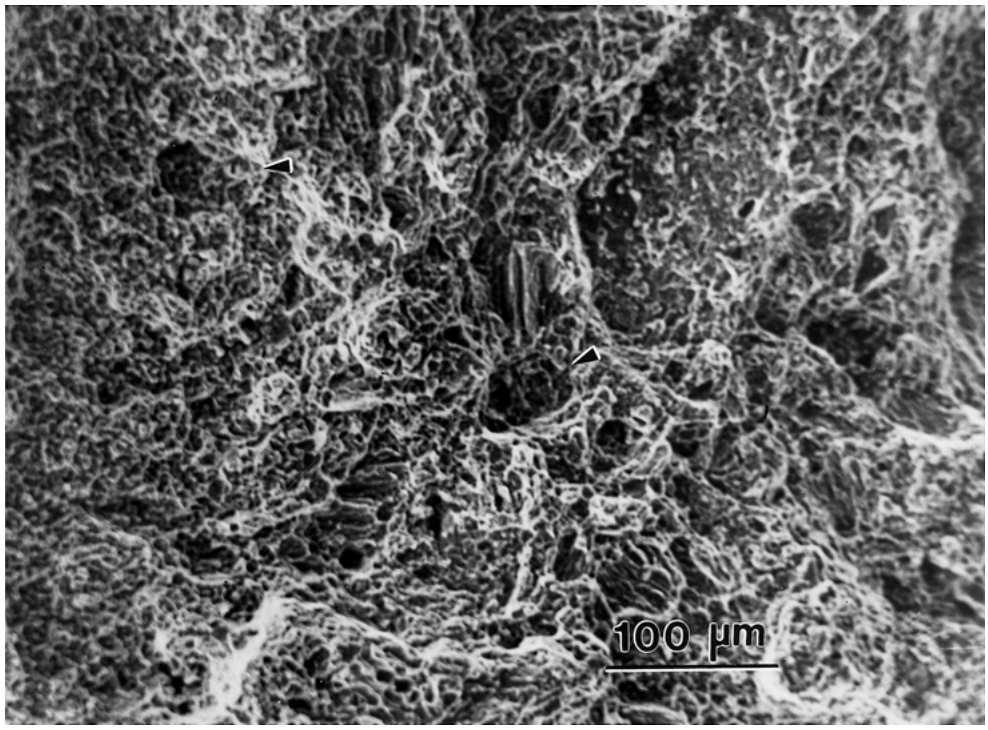

Figure 10 SEM fractograph showing considerable ductile-dimple structure in the eutectic matrix for a high fraction solids (18%) sample fractured outside the weld zone in the thermomechanical affected regime. Arrow notes primary (α-Mg) globule decohesion.

AM60 samples, their mechanical response after FSW exhibited no recognizable degradation.

4. Conclusions

The friction-stir welding of thin (0.15 cm), thixomolded plates of AM-60 magnesium alloy produced excellent welds with no apparent loss in strength or weld integrity. The 2-phase (α-Mg + $Mg_{17}Al_{12}$) work-piece or as-molded matrix characterized by α-Mg grains surrounded by the intermetallic $Mg_{17}Al_{12}$, with primary solid particle fractions of 3 and 18%, become a homogeneous, recrystallized, equiaxed grain structure (Mg + 6% Al) within the corresponding weld zones. This reprocessing of the thixomolded plates is also an indication of the potential for friction-stir processing of these complex microstructures where desirable. The ability to friction-stir weld thixomolded, net-shape products of AM60 can provide an energy efficient, environmentally attractive manufacturing assembly route for numerous product applications.

Acknowledgments

We are grateful for the provision of thixomolded products in this research program by Thixomat, Inc., Ann Arbor, MI, USA. The support of Steve LeBeau of Thixomat, Inc. is especially acknowledged. This research was supported in part by a U.S. Department of Energy Grant (DE-FC04-01AL67097; Amendment No., A0001) and a Murchison Endowed Chair at the University of Texas at El Paso. J.A.E. was also supported in part by a Graduate Assistantship through the UTEP Graduate School. We are grateful for the technical support of David Brown in the friction-stir welding, Lola Norton in performing the EDX analyses, and Prof. Roy Arrowood in tensile testing.

References

1. R. CARNAHAN *et al*, in "Magnesium Alloys and Their Applications," DGM Conference in Garmisch-Partenkircken, FRG, April 1992, edited by B. L. Mordike and F. Hehman, p. 69.
2. L. E. MURR, YING LI, E. TRILLO, B. M. NOWAK and J. C. MCCLURE, *Aluminum Trans.* **1**(1) (1999) 141.
3. *Idem., Mater. Tech. & Adv. Performance Mater.* **15** (1) (2000) 35.
4. K. V. JATA, M. W. MAHONEY, R. S. MISHRA, S. L. SEMIATIN and D. P. FIELDS (eds.), "Friction-Stir Welding and Processing" (The Minerals, Metals and Materials Society (TMS), Warrendale, PA, 2001).
5. T. NAGASAWA, M. OTSUKA, T. YOKOTA and T. UEKI, in "Magnesium Technology 2000," edited by H. I. Kaplan, J. Hryn and B. Clow (The Minerals, Metals, and Materials Society (TMS), Warrendale, PA, 2000) p. 383.
6. J. A. ESPARZA, W. C. DAVIS, E. A. TRILLO and L. E. MURR, *J. Mater. Sci. Lett.* **21** (2002) 917.
7. K. NAKATA, S. INOKI, Y. NAGANO, T. HASHIMOTO, S. JOHGAH and M. USHIO, *J. Japan Inst. of Light Metals* **51**(10) (2001) 528.
8. R. S. MISHRA, M. W. MAHONEY, S. X. MC FADDEN, N. A. MARA and A. K. MUKHERJEE, *Scripta Mater.* **42** (2) (2000) 163.
9. M. MAHONEY, R. S. MISHRA, T. NELSON, J. FLINTOFF and R. ISLANGALIEV, in "Frictional-Stir Welding and Processing" (The Minerals, Metals and Materials Society (TMS), Warrendale, PA, 2001) p. 183.
10. R. S. MISHRA and M. W. MAHONEY, *Mater. Sci. Forum* **375–359** (2001) 507.
11. F. CZERWINSKI, A. ZIELINSKA-LIPIEC, P. J. PINET and J. OVERBEEKE, *Acta Mater.* **49** (2001) 1225.
12. W. TANG, X. GUO, J. C. MCCLURE, L. E. MURR and A. NUNES, *J. Mater. Processing & Manuf. Sci.* **7** (1998) 163.
13. G. V. RAYNOR, "The Physical Metallurgy of Magnesium and its Alloys" (Pergamon Press, New York, 1959).
14. L. E. MURR, "Electron and Ion Microscopy and Microanalysis: Principles and Applications," 2nd ed. (Marcel Dekker, New York, 1991).

15. C. G. RHODES, M. W. MAHONEY, W. H. BINGEL, R. A. SPURLING and C. C. BAMPTON, *Scripta Mater.* **36** (1997) 69.
16. G. LIU, L. E. MURR, C.-S. NIOU, J. C. MCCLURE and F. R. VEGA, *ibid.* **37** (197) 355.
17. L. E. MURR, Y. LI, E. A. TRILLO, B. M. NOWAK and J. C. MCCLURE, *Aluminum Trans.* **1** (1) (1999) 141.
18. L. E. MURR, Y. LI, R. D. FLORES, E. A. TRILLO and J. C. MCCLURE, *Mater. Res. Innovations* **293** (1998) 150.
19. Y. LI, L. E. MURR and J. C. MCCLURE, *Mater. Sci. Engng.* A **271** (1999) 213.
20. Y. LI, E. A. TRILLO and L. E. MURR, *J. Mater. Sci. Lett.* **19**(12) (2000) 1047.
21. L. E. MURR, Y. LI, E. A. TRILLO and J. C. MCCLURE, *Mater. Tech. and Adv. Performance Mater.* **15**(1) (2000) 35.
22. R. A. PRADO, L. E. MURR, D. J. SHINDO and K. F. SOTO, *Scripta Mater.* **45** (2001) 75.
23. D. GHOSH, K. KANG, C. BACH, J. G. ROEMER and C. VAN SCHILT, in Proc. 34th Annual Conf. of Metallurgists of CIM, Vancouver, BC, 1995, p. 481.

Received 17 April
and accepted 29 October 2002